1 OF 1
AD
A053422

END
DATE
FILMED
6-78

DDC

1.0

4.5
5.0
5.6
6.3

2.8   2.5

3.2   2.2

3.6

1.1

4.0   2.0

1.8

1.25   1.4   1.6

MICROCOPY RESOLUTION TEST CHART
NATIONAL BUREAU OF STANDARDS-1963-A

AD A053422

AD No. ___
DDC FILE COPY
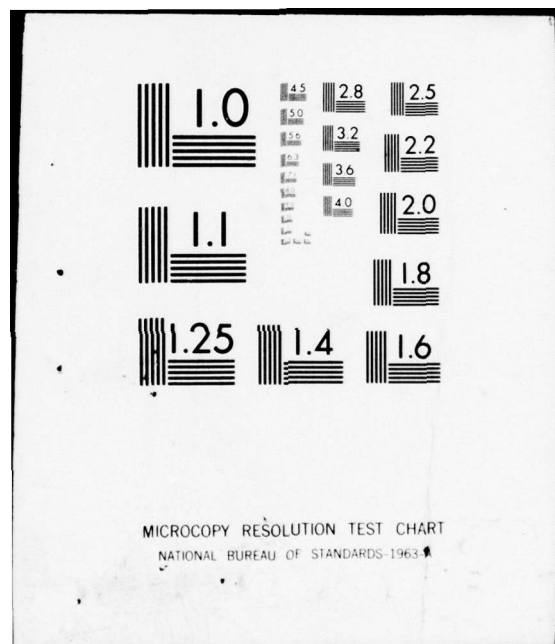
NWSC/CR/RDTR-73

SELF DIFFUSION IN CELLS AND TISSUES
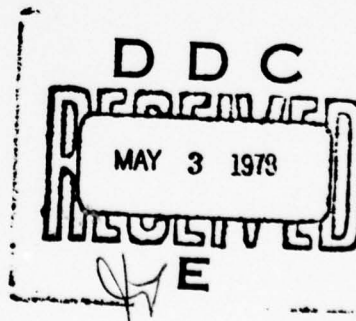   ANNUAL REPORT NO. 3

by
John E. Tanner, Jr.

Naval Weapons Support Center
Applied Sciences Department
Crane, Indiana 47522

1 October 1977

Final REPORT for Period 1 October 1976 to 30 September 1977

APPROVED FOR PUBLIC RELEASE: DISTRIBUTION UNLIMITED

D D C
RECEIVED
MAY 3 1978
E
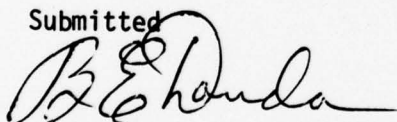
Prepared for
Office of Naval Research
Medical and Dental Science
Arlington, Virginia   22217

Submitted

B. E. DOUDA, Manager
Chemical Sciences Branch
Pyrotechnic Division
Applied Sciences Department

REPORT DOCUMENTATION PAGE		READ INSTRUCTIONS BEFORE COMPLETING FORM
1. REPORT NUMBER NWSC/CR/RDTR-73	2. GOVT ACCESSION NO.	3. RECIPIENT'S CATALOG NUMBER
4. TITLE (and Subtitle) SELF DIFFUSION IN CELLS AND TISSUES Annual Report No. 3		5. TYPE OF REPORT & PERIOD COVERED Annual Rept. no. 3 (Final) 1 Oct 1976 - 30 Sep 1977 6. PERFORMING ORG. REPORT NUMBER
7. AUTHOR(s) JOHN E. TANNER, Jr.		8. CONTRACT OR GRANT NUMBER(s) N00014-77-WR-70035
9. PERFORMING ORGANIZATION NAME AND ADDRESS Naval Weapons Support Center Applied Sciences Department Crane, Indiana 47522		10. PROGRAM ELEMENT, PROJECT, TASK AREA & WORK UNIT NUMBERS Task No. 207-013
11. CONTROLLING OFFICE NAME AND ADDRESS Office of Naval Research Medical and Dental Science Arlington, Virginia 22217		12. REPORT DATE 1 October 1977
		13. NUMBER OF PAGES 44
14. MONITORING AGENCY NAME & ADDRESS(if different from Controlling Office)		15. SECURITY CLASS. (of this report) UNCLASSIFIED
		15a. DECLASSIFICATION/DOWNGRADING SCHEDULE

16. DISTRIBUTION STATEMENT (of this Report)

APPROVED FOR PUBLIC RELEASE: DISTRIBUTION UNLIMITED

17. DISTRIBUTION STATEMENT (of the abstract entered in Block 20, if different from Report)

18. SUPPLEMENTARY NOTES

Reproduction in whole or in part is permitted for any purpose of the United States Government.

19. KEY WORDS (Continue on reverse side if necessary and identify by block number)

Biophysics
Diffusion
Nuclear Magnetic Resonance
Heat Flow

Nuclear magnetic resonance

20. ABSTRACT (Continue on reverse side if necessary and identify by block number)

A general treatment of time-dependent (transient) diffusion coefficients in a system of parallel planar barriers of arbitrary permeability has been performed, with emphasis on the results expected for NMR pulsed-field-gradient, spin-echo measurements. This is the first such derivation for permeable barriers of any geometry. The calculated distribution functions and diffusion coefficients are in agreement with expectations in most of the limiting cases tried, except that an unexplained (see reverse)

DD FORM 1473 EDITION OF 1 NOV 65 IS OBSOLETE
1 JAN 73
S/N 0102-014-6601

dependence of the diffusion coefficients on the magnitude of the field gradient was found. The application of the results to the interpretation of experimental results is discussed. This work has been accepted for publication by the Journal of Chemical Physics.

PREFACE

The computer facilities of the Data Processing Department of NAVWPNSUPPCEN Crane and at the Wrubel Computing Center of Indiana University were used for the computations performed here.

Thanks are due to Professor Andrew Lenard of Indiana University and Dr. Harold Sabbagh of NAVWPNSUPPCEN Crane for comments on the manuscript.

TABLE OF CONTENTS

LIST OF FIGURES

LIST OF TABLES

BACKGROUND

Magnetic field gradient NMR is well adapted to measuring diffusion
in colloidal systems, including biological cells, because the experi-
mental measurement times by this method are such that the distances
traveled by the molecules are of the same order as the dimensions
of the inhomogeneities of the system. The result is that the apparent
diffusion coefficients are dependent on the diffusion time. By vary-
ing this latter parameter the dimensions of the inhomogeneities as
well as the local diffusion coefficients within them can be obtained.

The maximum information is obtained by the use of the widest
possible range of diffusion times. In previously reported work, a
variety of recently developed techniques have been used to get a
much wider range of diffusion times than had been employed in earlier
studies of diffusion in biological materials.

The theory of the use of pulsed-field-gradient NMR to measure
intracellular self diffusion has been outlined in Annual Report No.
1[1] of this project, along with a description of the equipment assembled
to perform the measurements. A preliminary description of the results
of a series of measurements on various frog muscles was also given
there.

The experimental results were presented in full in Annual Report
No. 2[2] of this project, including diffusion and spin relaxation
measurements on frog muscles, red cells, yeast and E. coli. They

3

are presently being written for publication in the open literature.

Much of this work was presented at the 21st Annual Meeting of the Biophysical Society, February 15-18, 1977 in New Orleans.

Since then, a complete theoretical derivation of the relation between diffusion coefficients and diffusion time, as measured by an NMR pulsed-gradient experiment, has been performed. The results constitute the present report. This work has been accepted for publication by the Journal of Chemical Physics.

INTRODUCTION

When diffusional motion is observed in an inhomogeneous system
the degree of mobility of any particular substance appears to depend
on the length of the observation time. At short enough times a wide
spectrum of mobilities may be observed, corresponding to a variation
in local viscosities. At long enough observation times a uniform
averaged mobility is observed because the substance has an opportunity
to repeatedly sample all of the different environments.

One particular type of system which occurs frequently is a set
of barriers in an otherwise homogeneous medium. The amount of sub-
stance within the barrier at any one time may be quite small. In
that case, if diffusion is observed over a short enough time, very
little of the substance experiences the effect of the barriers, and
the observed motion is characteristic of the medium alone. As the
time of observation is extended, more of the substance is reflected
at barriers; and thus, its total displacement is less than would
have been the case without the barriers. We say that the apparent
(transient) diffusion coefficient $\underline{D}(\underline{t})$ decreases, although the total
displacement generally has increased. In the limit of long obser-
vation times the apparent diffusion coefficient asymptotically
approaches a new value which depends on the permeability and the
geometric arrangement of the barriers as well as the viscosity of
the medium.

Magnetic-field-gradient, spin-echo methods have been increasingly employed for measurements in this type of system when the spacing of the barriers corresponds to colloidal dimensions (for reviews, see references 3 and 4). This is because the experimentally accessible range of diffusion times corresponds to distances of the order of colloidal dimensions, so that diffusion can be observed over a range of times such that a considerable change in apparent diffusion coefficient may be observed.

By fitting a set of such diffusion measurements to mathematical functions appropriate to the geometry of the system under observation it is possible to extract the system variables, i.e., the local diffusion coefficients, and the barrier spacings and permeabilities.

The appropriate mathematical functions are usually quite complicated even for simple geometries, however. Derivations are available only for homogeneous media bounded by spherical,[5,6] cylindrical,[5,7] or planar[5,8-11] barriers which are impermeable. The author is aware of no formula for any geometry of periodic barriers of arbitrary permeability. Nevertheless, such geometries are present in many interesting experimental systems. The outer membrane of most cells is highly permeable to water and to many other substances. The continuous phase of an emulsion and open pore rocks, minerals, and plastic foams are also systems containing barriers which may be penetrated or bypassed.

6

A few suggestions have been made of approximate methods for handling data from such systems, based on a superposition of the short time and long time limits of the diffusion coefficient, $\underline{D}(o)$ and $\underline{D}(\infty)$ respectively, according to an equation

$$\underline{D}(\underline{t}) = f(\underline{t}) \cdot \underline{D}(o) + [1-f(\underline{t})] \cdot \underline{D}(\infty) \qquad (1)$$

where $f(\underline{t})$ is assumed independent of $\underline{D}(\infty)$.[4,12] Derivations such as in references 5-11 give $f(\underline{t})$ for $\underline{D}(\infty) = 0$. We may ask whether the same $f(\underline{t})$ could be used in Eq.(1) when $\underline{D}(\infty) \neq 0$.

We report here an exact derivation of $\underline{D}(\underline{t})$ for one special case, and we show that it cannot be approximated as in Eq.(1). The chosen case is one-dimensional diffusion through equally spaced barriers of equal but arbitrary permeability, $\underline{p}$. A finite, constant diffusion coefficient $\underline{D}(o)$ exists in the intervening spaces. In three dimensional space the barriers would consist of parallel planes normal to the direction in which the diffusional observations are made, see Figure 1. Non-absorbing barriers parallel to the direction of observation would have no effect on motion in this direction; therefore, the geometry chosen can also represent cubical barriers. It also may be expected to approximate to first order the geometry of many practical systems of regularly spaced barriers.

7

The results obtained below apply equally well to the case of transient heat flow in a stack of planar slabs with finite contact resistance at the interfaces and a planar source. In that case, which we will not discuss further, one should replace $\underline{D}(o)$ by $\alpha = \underline{k}/\underline{c}$, $\underline{p}$ by $\underline{h}/\underline{c}$, and ρ by the temperature, where α is the thermal diffusivity, $\underline{k}$ is the thermal conductivity, $\underline{c}$ is the heat capacity per unit volume, $\underline{h}$ is the "radiation constant" at the interface, and ρ is the spin distribution function.

DERIVATION

Our purpose is to calculate the diffusion coefficient in the chosen system as it would be measured by a spin-echo NMR experiment where the echo is attenuated by the application of pairs of field gradient pulses of magnitude $\underline{g}$, and of duration δ, short compared to their separation, Δ. It has been shown that in such an experiment[13] Δ represents the diffusion time, $\underline{t}$, and that the relative echo height, $\underline{R}$, is given by[6,8]

$$\underline{R}(\underline{t}) = \int_{-\infty}^{\infty} \int_{-\infty}^{\infty} \rho(\underline{x}_0 | \underline{x}, \underline{t}) \cdot \cos[\gamma\delta\underline{g}(\underline{x}-\underline{x}_0)]\underline{dxdx}_0, \qquad (2)$$

where ρ is the conditional probability for the arrival at $\underline{x}$, at time $\underline{t}$ of nuclei which originated at $\underline{x}_0$ at $\underline{t} = 0$. $\underline{R}$ is defined as the ratio of signal (echo) strengths with and without the gradient, and is less than unity if diffusion is taking place. γ is the nuclear gyromagnetic ratio.
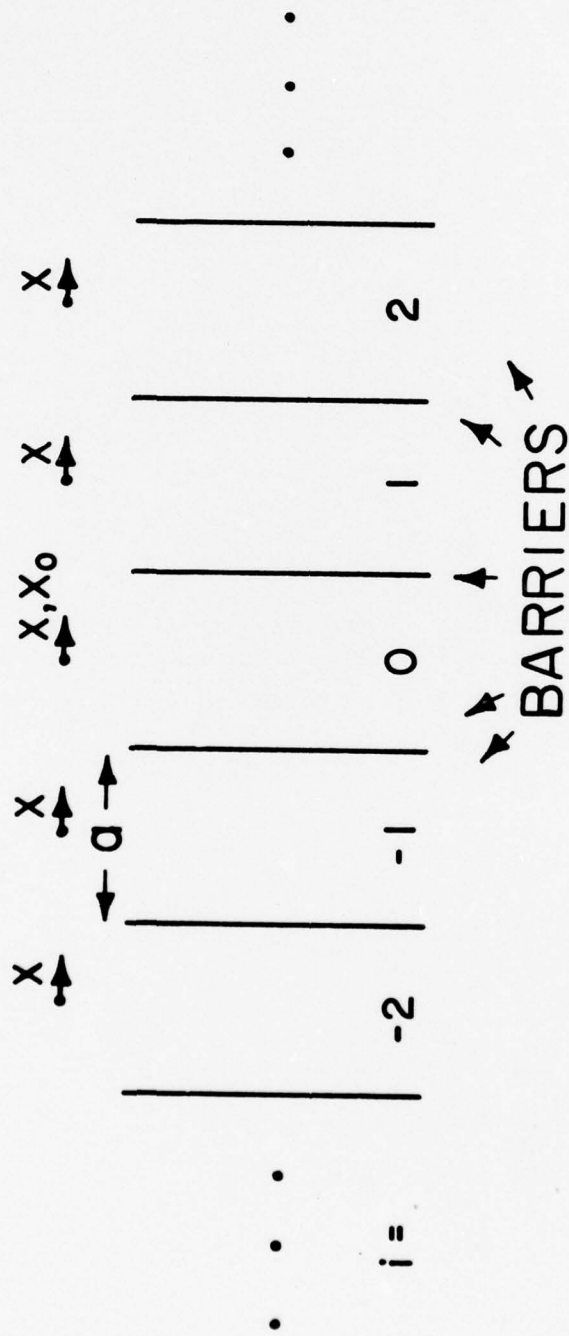
8

Fig. 1. A system of regularly spaced planar barriers. The location of the instantaneous source, $\underline{x}_0$, is measured from the center of the region $\underline{i} = 0$; whereas $\underline{x}$ is measured from the center of the region under consideration.

9

In a homogeneous system the diffusion coefficient is obtained from[13]

$$\ln \underline{R}(\underline{t}) = -\gamma^2 \underline{Dg}^2 \delta^2 \underline{t}. \tag{3}$$

Assuming no prior knowledge of the inhomogeneity of our system we combine Eq.(2) and Eq.(3) to define a transient "apparent" diffusion coefficient, $\underline{D}(\underline{t})$.

It is also informative to define the transient diffusion coefficient in a different way, by analogy to the Einstein relation, as $\overline{(\underline{x}-\underline{x}_0)^2} = 2\underline{D}(\underline{t}) \cdot \underline{t}$. Averaging over $\underline{x}_0$ we then have:

$$\underline{D}(\underline{t}) = (1/2\underline{t})\int_{-\infty}^{\infty} \int_{-\infty}^{\infty} \rho(\underline{x}_0 | \underline{x},\underline{t}) \cdot (\underline{x}-\underline{x}_0)^2 \underline{dxdx}_0 \tag{4}$$

Both Eq. (3) and Eq. (4) will be used, and the results compared.

For a theoretical derivation of either case we need an expression for ρ. Formulas from the literature,[14,15] valid for composite systems with a finite number of layers, have been adapted to our case of interfaces (barriers) of equal spacing and permeability. Provided $\underline{x}_0$ is within the system, and $\underline{t}$ is small enough so that ρ is negligible in the outer layers, the numerical results should be the same as for an infinite number of layers. The resulting distribution function is:

$$\rho(\underline{x}_0 | \underline{x},\underline{t}) = \sum_{\underline{n}=1}^{\infty} \left[\frac{\underline{X}_{on}(\underline{x}_0) \cdot \underline{X}_{in}(\underline{x})}{\sum_{\text{all } \underline{i}} \int_{\underline{i}\text{th}} \underline{X}^2_{in}(\underline{x})\underline{dx}} \exp(-\beta_{\underline{n}}^2 \underline{D}(o) \cdot \underline{t}) \right] \tag{5}$$

10

Here $\underline{X}_{in}$ are an infinite set of eigenfunctions of $(\partial^2/\partial\underline{x}^2 + \beta_{\underline{n}}^2)\ \underline{X}_{in} = 0$, discontinuous at the barriers, and of the form $\underline{X}_{in} = \underline{c}_{in}\cos\beta_{\underline{n}}\underline{x} + \underline{d}_{in}\sin\beta_{\underline{n}}\underline{x}$. The layers are numbered by $\underline{i}$ (see Figure (1)), and the subscript "o" refers to the layer in which $\underline{x}_o$ occurs. The functions satisfy the orthogonality relation $\displaystyle\sum_{\text{all } i} \int_{i\text{th}} \underline{X}_{in} \cdot \underline{X}_{im} dx = 0,\ \underline{n} \neq \underline{m}$.

The boundary conditions are that for each interface

$$\partial\underline{X}_{\underline{i}}/\partial\underline{x} = \partial\underline{X}_{\underline{i}+1}/\partial\underline{x} \qquad \text{and} \qquad (6)$$

$$\underline{p} \cdot (\underline{X}_{\underline{i}+1} - \underline{X}_{\underline{i}}) = \underline{D}(o) \cdot \partial\underline{X}_{\underline{i}}/\partial\underline{x} \qquad (7)$$

At the outer faces we arbitrarily assume diffusion into a sink, so that one or the other of the $\underline{X}$ on the left side of Eq.(7) is zero, and Eq.(6) does not apply. These boundary conditions form a set of homogeneous simultaneous equations from which sets of $\underline{c}$, $\underline{d}$, and β are obtained.

For substituting Eq.(5) into Eqs.(2) or (4), a great simplification of the algebra and of the numerical computations was accomplished by defining the coordinate so as to let $\underline{x}$ represent the distance from the middle of the same layer, in units of $\underline{a}$, as in Figure 1. The term $(\underline{x}-\underline{x}_o)$ in Eqs.(2) and (4) then became $(\underline{x}+\underline{i}-\underline{x}_o)$, where $\underline{i}$ is the number of layers from the one containing $\underline{x}_o$ to the one containing $\underline{x}$.

11

The integration over $\underline{x}$ was carried out for each layer separately, then summed over all layers. If a large enough number of layers is chosen so that $\rho(\underline{x}_o|\underline{x}, \underline{t})$ is negligible in the outermost layers at the longest times, $\underline{t}$, to be considered, then the system has translational symmetry, and the integration over $\underline{x}_o$ need be performed only over one layer, for convenience the center layer of an odd-numbered stack.

The final expression for the spin echo height is then:

$$\underline{R}(\underline{t}) = \sum_{\underline{n}} \left[(\underline{Z}+\underline{Y})(\underline{Z}-\underline{Y}) \sum_{\underline{i}} (\underline{c}_o\underline{d}_{\underline{i}} - \underline{c}_{\underline{i}}\underline{d}_o) \sin\theta\underline{i} \right.$$

$$\left. + (\underline{Z}+\underline{Y})^2 \underline{c}_o \sum_{\underline{i}} \underline{c}_{\underline{i}}\cos\theta\underline{i} + (\underline{Z}-\underline{Y})^2 \underline{d}_o \sum_{\underline{i}} \underline{d}_{\underline{i}}\cos\theta\underline{i} \right](1/\underline{A}_{\underline{n}})$$

$$\exp(-\beta_{\underline{n}}^2 \underline{T}) \tag{8}$$

where $\underline{Z} = \dfrac{\sin[(\theta+\beta_n)/2]}{\theta+\beta_{\underline{n}}}$, $\underline{Y} = \dfrac{\sin[(\theta-\beta_n)/2]}{\theta-\beta_{\underline{n}}}$, $\theta = \gamma\delta g a$, $\underline{T} = \underline{D}(o)\underline{t}/\underline{a}^2$, and

$$\underline{A}_{\underline{n}} = (1/2) \sum_{\underline{i}} (\underline{c}_{\underline{i}}^2 + \underline{d}_{\underline{i}}^2) + (1/\beta_{\underline{n}})\sin(\beta_{\underline{n}}/2)\cos(\beta_{\underline{n}}/2) \sum_{\underline{i}} (\underline{c}_{\underline{i}}^2 - \underline{d}_{\underline{i}}^2).$$

$\underline{D}(\underline{t})$ is then calculated from Eq.(3).

The alternate expression for $\underline{D}(\underline{t})$ as defined by Eq.(4) is:

$$\underline{D}(\underline{t}) = (1/2\underline{T}) \sum_{\underline{n}} (\underline{I}_{\underline{n}}/\underline{A}_{\underline{n}})\exp(-\beta_{\underline{n}}^2 \underline{T}), \tag{9}$$

where $\underline{A}_{\underline{n}}$ is as before, and

$$\underline{I}_{\underline{n}} = (\underline{c}_0/2\underline{b}_{\underline{n}}^4)\ \sin\underline{b}_{\underline{n}}[\underline{b}_{\underline{n}}^2\sin\underline{b}_{\underline{n}}-2(\sin\underline{b}_{\underline{n}}-\underline{b}_{\underline{n}}\ \cos\underline{b}_{\underline{n}})]\sum_{\underline{i}}\ \underline{c}_{\underline{i}}$$

$$-(\underline{d}_0/\underline{b}_{\underline{n}}^3)\ \sin\underline{b}_{\underline{n}}[\sin\underline{b}_{\underline{n}}-\underline{b}_{\underline{n}}\cos\underline{b}_{\underline{n}}]\sum_{\underline{i}}\underline{c}_{\underline{i}}\ \underline{i}$$

$$+(\underline{c}_0/\underline{b}_{\underline{n}}^2)\ \sin^2\underline{b}_{\underline{n}}\sum_{\underline{i}}\ \underline{c}_{\underline{i}}\underline{i}^2$$

$$-(\underline{d}_0/2\underline{b}_{\underline{n}}^4)[\sin\underline{b}_{\underline{n}}-\underline{b}_{\underline{n}}\cos\underline{b}_{\underline{n}}]^2\sum_{\underline{i}}\ \underline{d}_{\underline{i}}\quad,$$

$$+(\underline{c}_0/\underline{b}_{\underline{n}}^3)\sin\underline{b}_{\underline{n}}[\sin\underline{b}_{\underline{n}}-\underline{b}_{\underline{n}}\cos\underline{b}_{\underline{n}}]\ \sum_{\underline{i}}\ \underline{d}_{\underline{i}}\underline{i},$$

where $\underline{b}_{\underline{n}} = \beta_{\underline{n}}/2$.

NUMERICAL RESULTS

Using Eqs. (8) and (9) a large number of numerical evaluations were performed, mostly for a 19-region system, although a smaller number of computations were also performed for 1-, 3-, 5-, 7-, and 41-region systems. All of the results presented below pertain to 19 layers, unless otherwise noted.

13

The Distribution Function, $\rho(\underline{x}_0 | \underline{x}, \underline{t})$

Numerical calculations of ρ are not necessary to the calculation of apparent diffusion coefficients since these may be obtained directly from Eq. (8) or Eq. (9). Nevertheless, these distribution functions are interesting, and their evaluation afforded checks on a part of the procedure.

Distributions for an instantaneous source at the center $(\underline{x}_0 = 0)$ of one region are presented in Figure 2 for different values of the reduced permeability, $\underline{P} \equiv a\rho/\underline{D}(o)$ and of the reduced time, $\underline{T} \equiv \underline{D}(o) \cdot \underline{t}/\underline{a}^2$. Since the functions are symmetric about $\underline{x}_0$ the curves are reproduced only on one side of the region containing the source. One example is given for an assymetrically placed $\underline{x}_0$ in Figure 3.

The results are in many ways as expected. The functions decrease monotonically on both sides of a single maximum, and are discontinuous at the barriers.

The maximum of ρ remains at the center for $\underline{x}_0 = 0$, or moves eventually toward the center if $\underline{x}_0 \neq 0$. A number of numerical calculations of the slopes on both sides of an interface showed that Eqs. (6) and (7) are satisfied; and calculations of ρ at several closely spaced $\underline{T}$ showed that $\delta^2 \rho / \delta \underline{x}^2 = \delta \rho / \delta \underline{T}$ is satisfied in the regions between the barriers. Each of these checks was done for several values of $\underline{P}$ and of $\underline{T}$.

14

Fig. 2(a). Distribution of randomly diffusing particles from an
instantaneous source at the center of the middle
layer of a 19-layer system at reduced times $\underline{T}$ = .01,
.1, 1, 10, as labeled, at reduced permeability $\underline{P}$ = ∞.

15

Fig. 2(b). Distribution of randomly diffusing particles from an
instantaneous source at the center of the middle
layer of a 19-layer system at reduced times $\underline{T}$ = .01,
.1, 1, 10, as labeled, at reduced permeability $\underline{P}$ = 2.0.

16

Fig. 2(c). Distribution of randomly diffusing particles from an
instantaneous source at the center of the middle
layer of a 19-layer system at reduced times $\underline{T}$ = .01,
.1, 1, 10, as labeled, at reduced permeability $\underline{P}$ = 0.5.

17

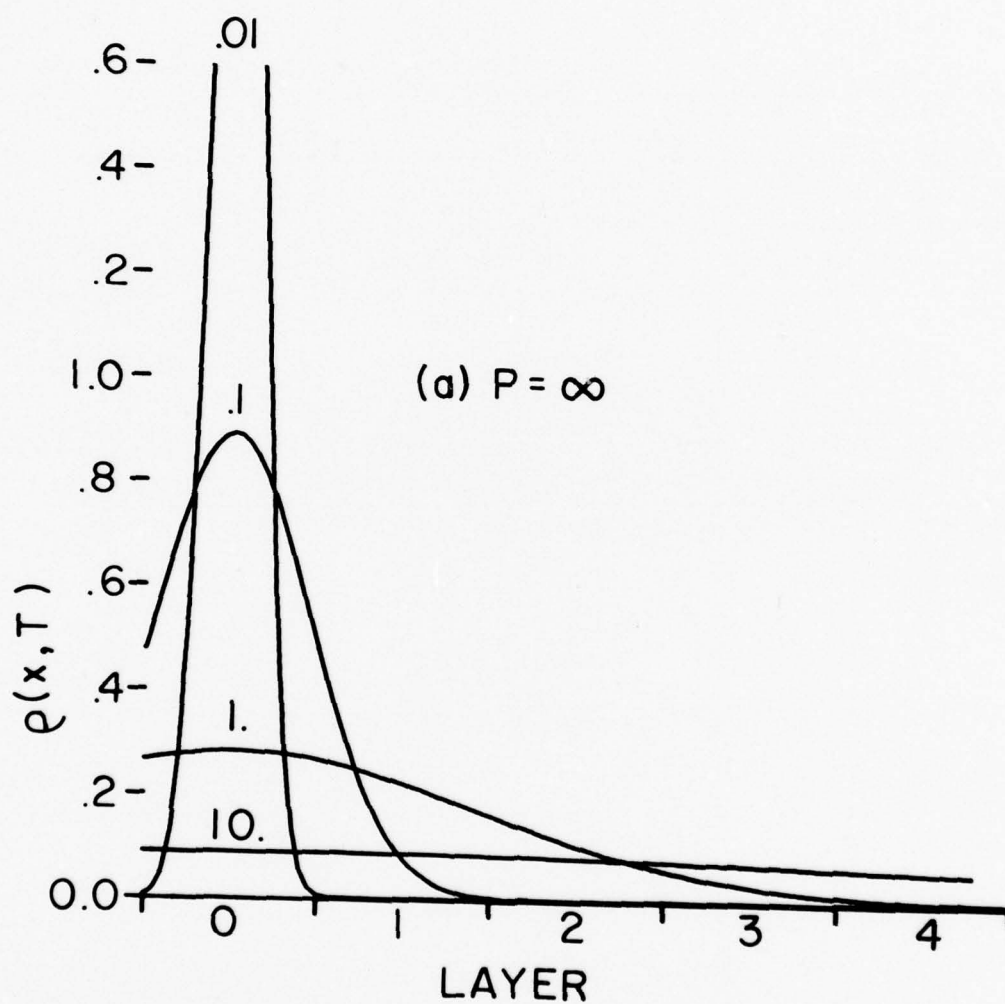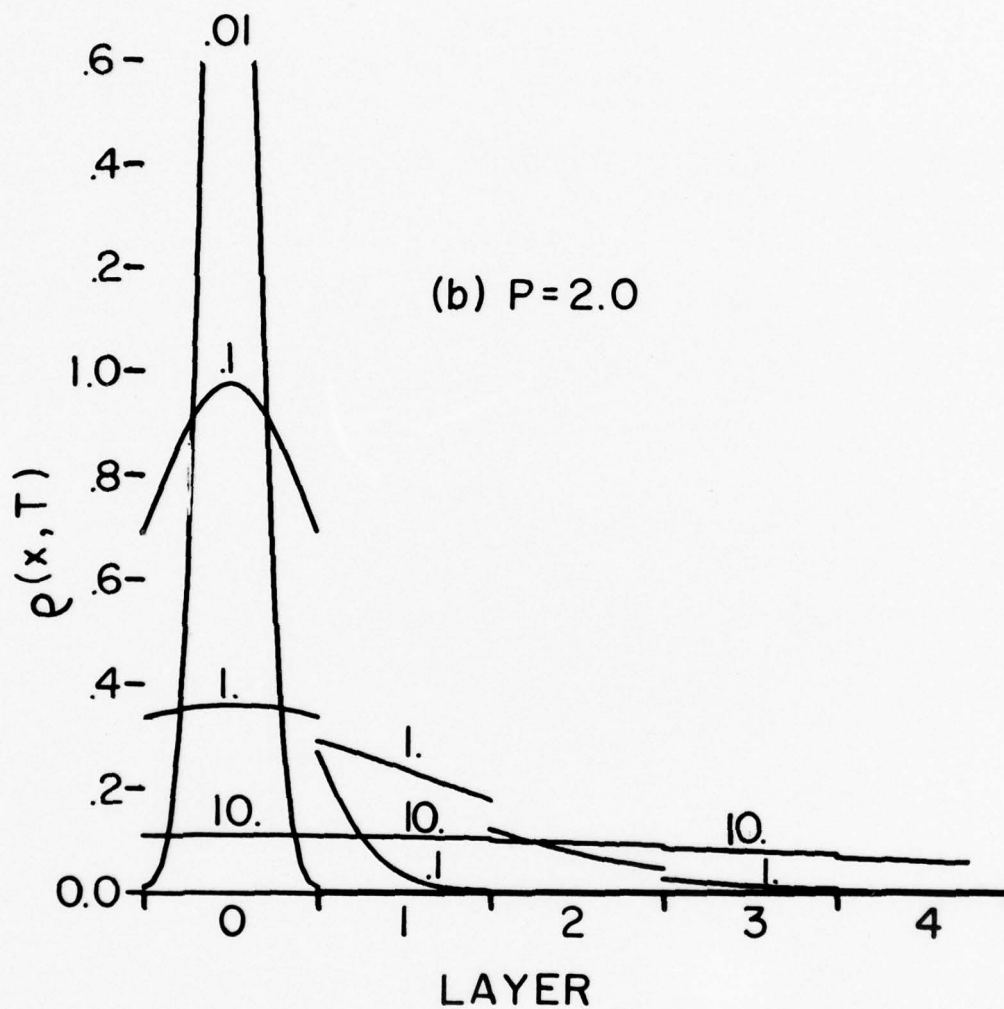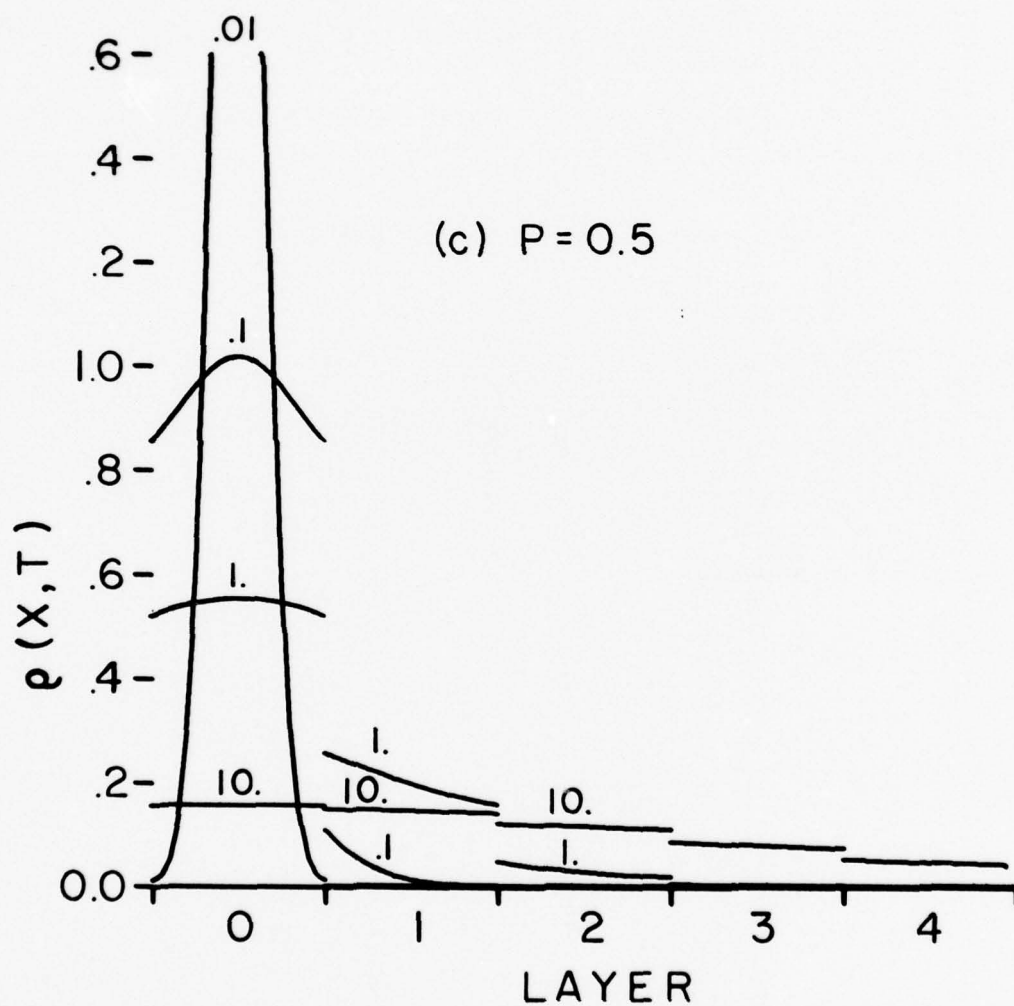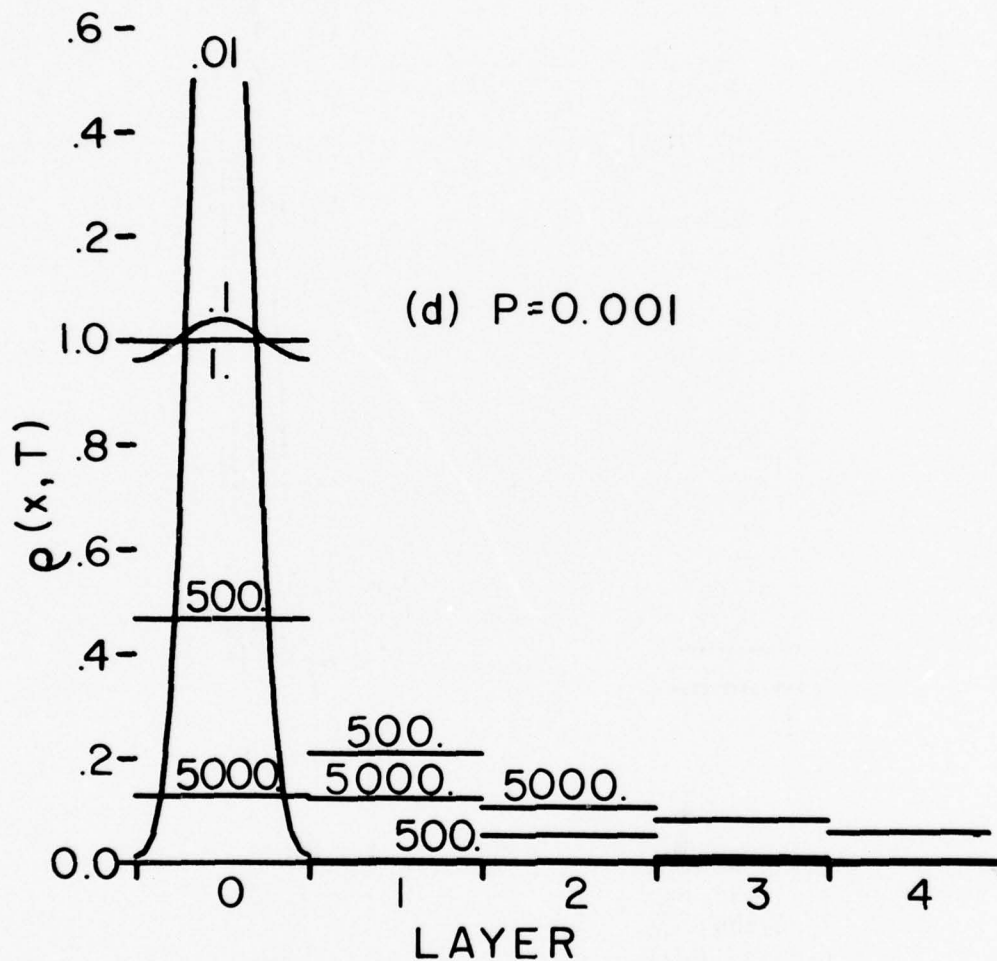Fig. 2(d). Distribution of randomly diffusing particles from an
instantaneous source at the center of the middle
layer of a 19-layer system at reduced times $\underline{T}$ = .01,
.1, 1, 500, and 5000, as labeled, at reduced
permeability $\underline{P}$ = 0.001.

18
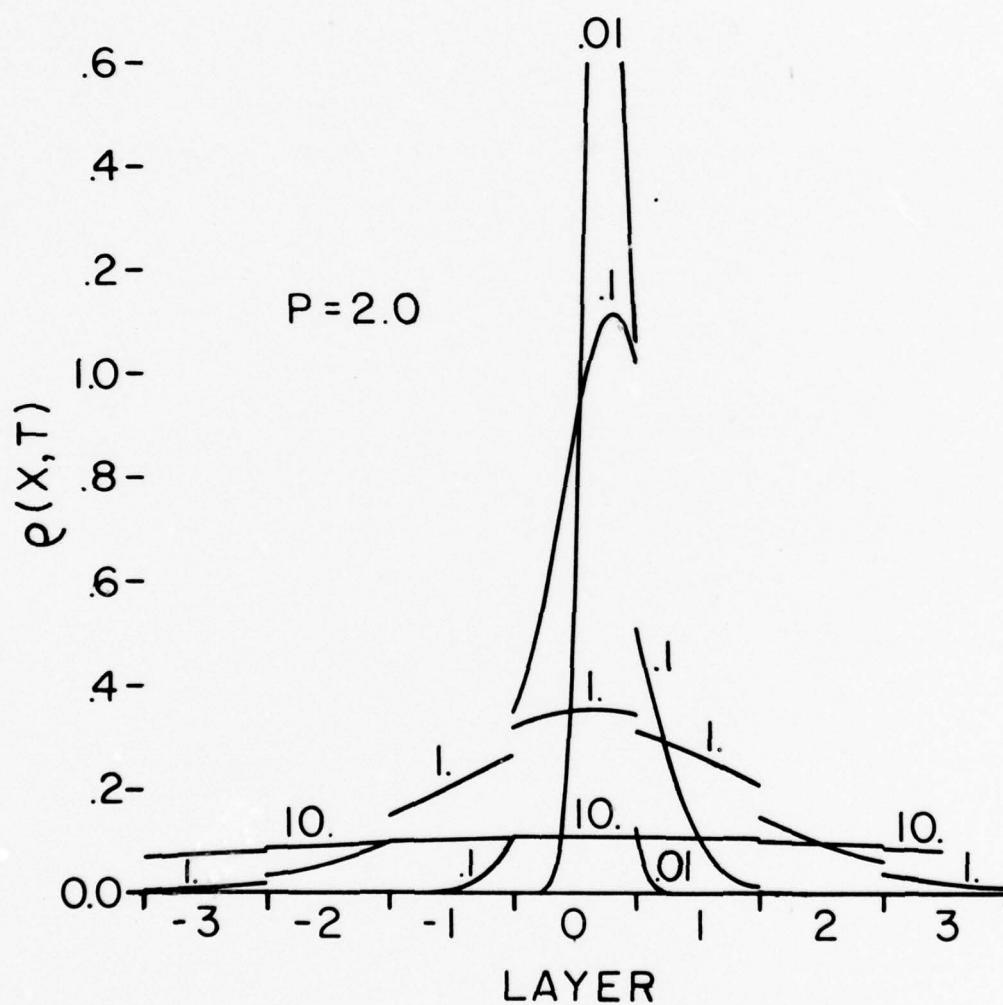
Fig. 3. Distribution about an assymetrically-placed instantaneous source located at $\underline{x}_0 = 0.25$. Times are labeled as in Figure 2.

The form has the appearance of a Gaussian or of segments thereof. For the case of arbitrary P and very short T, where the distribution function is small at the edges of the center region, or for the case of arbitrary T but infinite P (no barriers) the numerical results quantitatively fit the function

$$\rho = 1/(4 \pi \underline{T})^{1/2} \exp[-\underline{x}^2/4\underline{T}] \tag{10}$$

In the case of zero permeability the results for any $(\underline{x}_0, \underline{T})$ agree accurately with results derived earlier from a different starting formula.[8,9] It is of interest to note that for this limiting case ρ may also be accurately constructed by repeated total reflection of Eq.(10) at the barriers.

For finite permeability and diffusion time ρ is not Gaussian, nor can it be constructed by any simple scheme of partial reflections of a Gauss function at the barriers. This can be shown from the boundary conditions, Eqs. (6) and (7).

Finally, it was found that the numerical values at the midpoints of the regions for the case $\underline{P} = 0.001$ do not follow either a Gaussian or a binomial distribution, but seem to approach them as $\underline{T}$ increases.

Diffusion Coefficients

Here we present diffusion coefficients calculated for a wide range of barrier permeabilities, of diffusion times, and of the gradient strength parameter $\Theta = \gamma \underline{g} \delta \underline{a}$. With the 19-region system

20

considered, it was possible to obtain diffusion coefficients well
into the range at long diffusion times where $\underline{D}(\underline{t}) \approx \underline{D}(\infty)$, without
violating the condition that the effects of the outer boundaries be
small.

In Figure 4a we present calculated echo heights $\underline{R}(\underline{t})$ versus
reduced diffusion time for several values of the reduced barrier
permeability. This is the form in which experimental spin-echo
diffusion results are typically presented. For low barrier perme-
abilities ($\underline{P} < 1$) it is the most useful type of plot for deciding whether
the experimental diffusion time has been extended to long enough
values so that $\underline{D}(\infty)$ can be approximated.

The curves all approach the same limiting slope as $\underline{T} \to 0$, and they
appear to approach various smaller limiting slopes as $\underline{T} \to \infty$, though we
will see later that this latter is true only for $\theta < 1$. The chord to
the origin from any point is proportional to the apparent diffusion
coefficient at this time as defined by Eq.(3). For a convenient
comparison these diffusion coefficients are plotted on the same time
scale in Figure 4b. When $\underline{P} = 0$, then $\underline{R}$ becomes independent of $\underline{D}(o)$
at long $\underline{T}$, and is determined only by the barrier spacing, according
to[8,9] $\underline{R}(\infty) = 2(1 - \cos\theta)/\theta^2$.

In Figure 5 the diffusion coefficients are plotted versus the
logarithm of the diffusion time in order to cover a larger range of
the latter. A small value of θ is chosen. For $\underline{T} \to 0$, $\underline{D}(\underline{t})/\underline{D}(o)$ appears

21
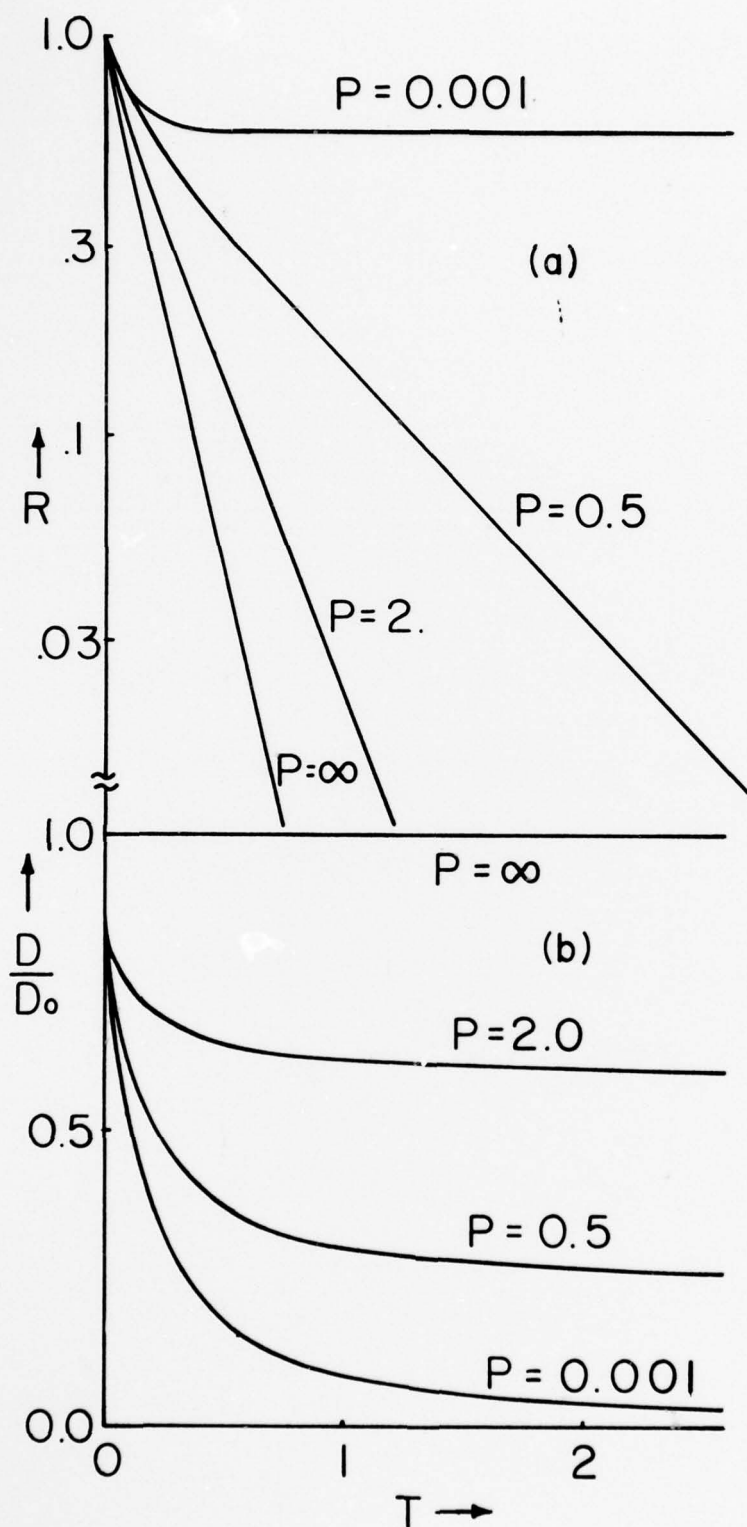
Fig. 4. (a) Semi-log plot of echo height, R, versus reduced diffusion
time for θ = 2.5, at the reduced permeabilities indicated. (b)
Relative diffusion coefficients on the same time scale as for
the parameters of (a).

22
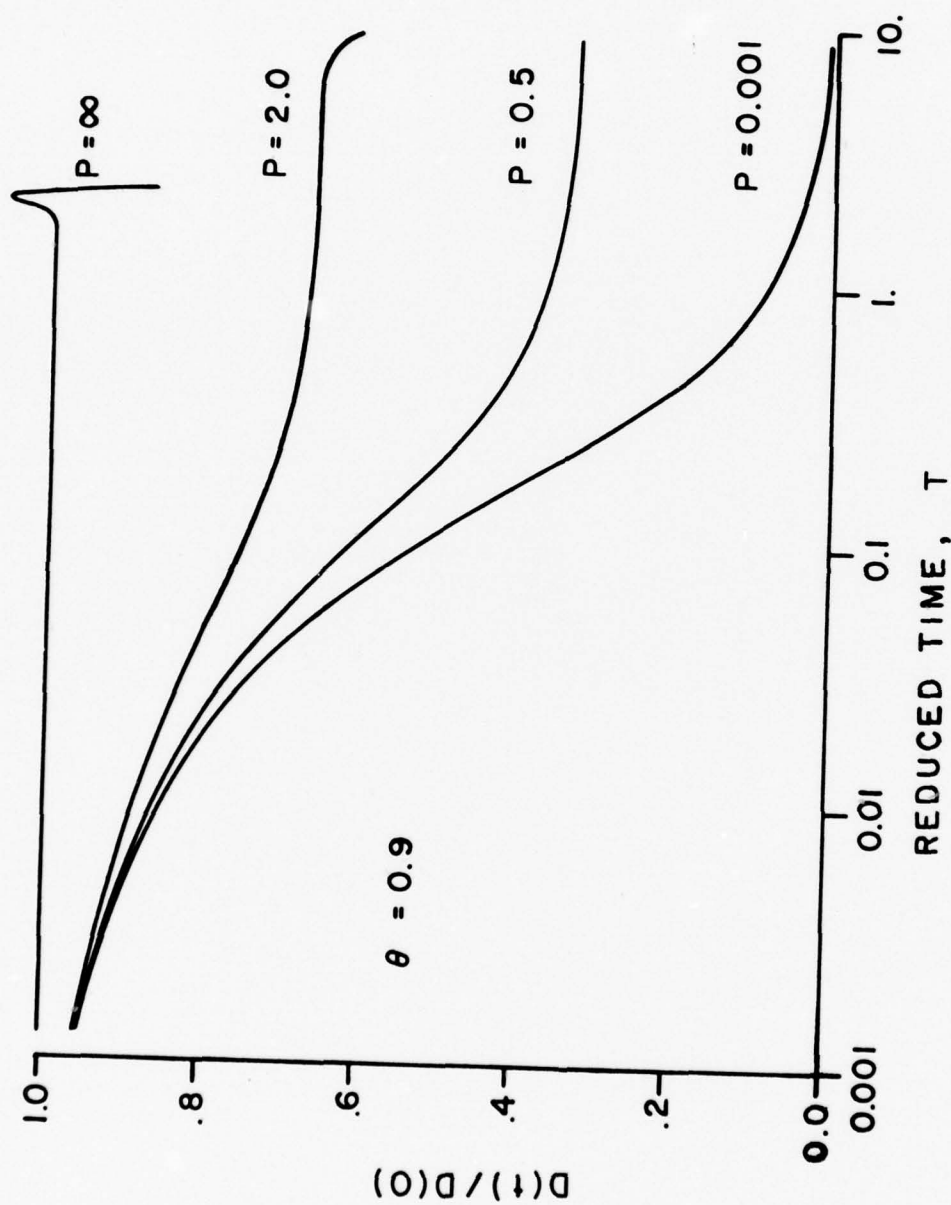
Fig. 5. Relative diffusion coefficient versus reduced diffusion time at several values of the reduced permeability, for a small value of Θ.

23

to approach unity, as expected. At long diffusion times it is verified numerically that the assymptotes satisfy

$$\underline{D}(o)/\underline{D}(\infty) = 1 + 1/\underline{P}, \qquad \text{for } \theta \to 0. \qquad (11)$$

This is a relation readily derived for the case of steady state diffusion from one side to the other in a system such as ours, and where $\underline{D}(\infty)$ would represent an overall diffusion coefficient, and $\underline{D}(o)$ an intrabarrier diffusion coefficient.

A close examination of the two curves for finite permeability, $\underline{P} = 0.5, 2$, shows that they are not even approximately linear combinations of the curves for $\underline{P}=0,\infty$. Therefore, the diffusion coefficients for a system of permeable barriers cannot be calculated by a simple superposition of results for impermeable barriers with results for no barriers, as in Eq.(1). It appears that the drop in diffusion coefficient takes place at progressively earlier times as the permeability increases. Note that the curves for $\underline{P}=2,\infty$ break away at the longest time, where the effect of outer boundaries has become important. To obtain useful results in this region we would have to consider a larger number of layers.

In Figure 6 (solid lines) we find that the NMR diffusion coefficient as defined by Eqs.(3) and (4) is not solely determined by the system parameters $(\underline{D}(o), \underline{a}, \underline{p})$ and the diffusion time, but also by the strength of the field gradient used to make the measurement. Although

24

REDUCED TIME, T
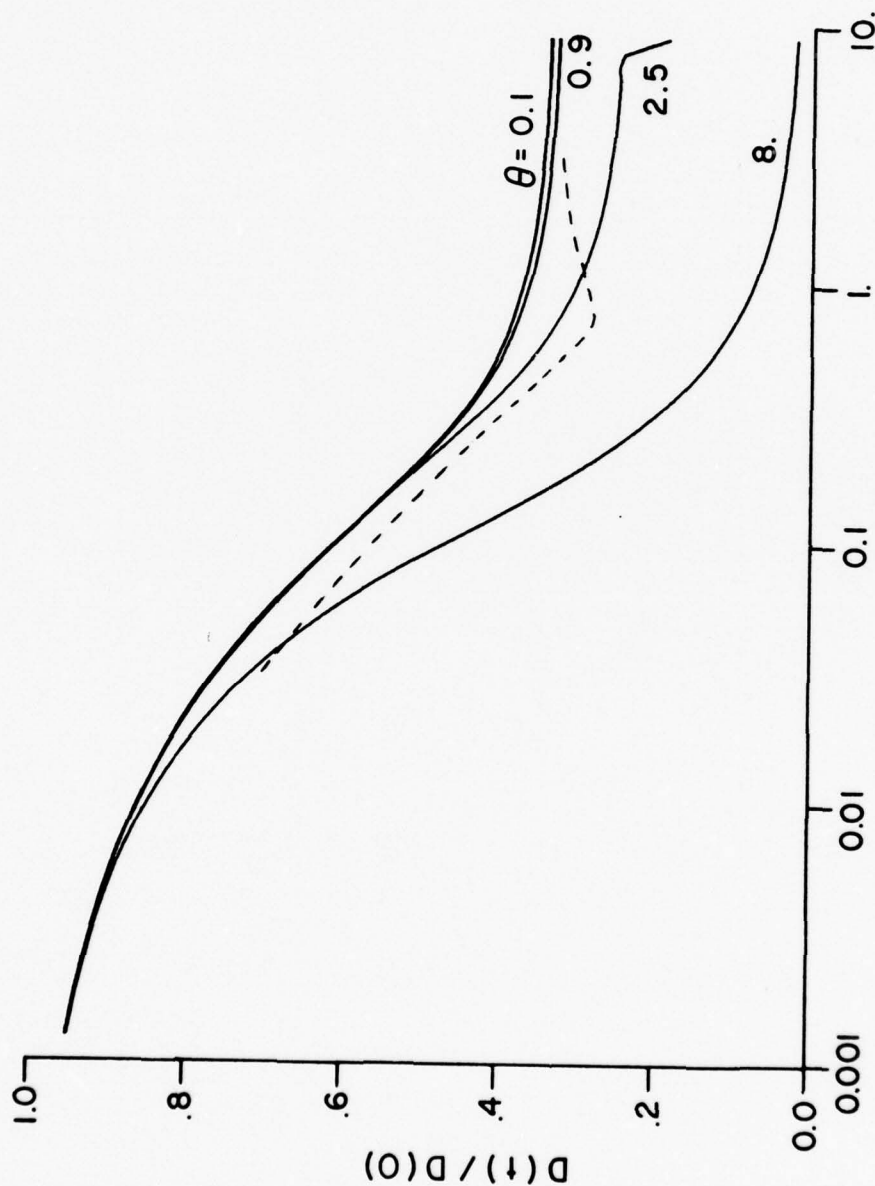
Fig. 6. Relative diffusion coefficient versus reduced diffusion time for $P = 0.5$. The solid curves are at the indicated values of Θ. The curve at $\Theta = 0.1$ coincides with the curve calculated from Eq. (9), using the Einstein definition of $\underline{D}(\underline{t})$. The dashed curve is for a variable Θ, as explained in the text.

25

the NMR $\underline{D}(\underline{t})$ becomes independent of Θ and also agrees with the Einstein $\underline{D}(\underline{t})$ as defined by Eq.(4) when Θ approaches zero, $\underline{D}(\underline{t})$ for the NMR case becomes strongly Θ-dependent where $\Theta>1$. This is true for all permeabilities except in the limit $\underline{P}\rightarrow\infty$. The variation of $\underline{D}(\underline{t})$ with Θ is generally monotonic except for a few small regions of (Θ, T, P) space where either $\underline{R}$ or $\underline{D}$ increases with increasing Θ.

It is unfortunate for evaluating experimental results that the strong Θ-dependence occurs in a range of Θ which is expected for typical experimental systems, such as those of Table I. The fact that the values of $\underline{D}$ at larger Θ go below the expected limits at long time as calculated by Eq.(11) is even more troublesome. It is physically unreasonable either that $\underline{D}$ should increase as $\underline{T}$ is increased beyond the range presented in the figures or that $\underline{D}(\infty)$ should be less than as calculated from Eq.(11).

It may be asked whether this theoretical result is an artifact of the particular geometry chosen or of its ideal regularity. A satisfactory answer cannot be given here, and awaits calculations with systems of other geometries. It is the author's belief that it is the results for small Θ which will more likely be approximated when calculations with other geometries are performed, and that these results should be more trustworthy for application to experimental systems in the meantime.

TABLE I

Approximate range of parameters in typical pulsed gradient experiments on colloidal systems. State-of-the-art equipment assumed to include capability for stimulated echo and alternating gradient pulse sequences, for time averaging (used at long t), and for gradients to 500 G/cm.

Example	Single Cell	Muscle Cell	Oil Droplet
System parameters			
a, μm	3	50	10
$D(o)$, cm^2/sec x10^5	0.5	1.5	0.01
$D(\infty)/D(o)$	0.4	0.6	0
T_2, msec	40	50	50
T_1, msec	500	1000	50
Experimental parameters			
t, msec	0.5 to 500	0.5 to 2000	1 to 60
T	0.03 to 30	.0003 to 1.2	.0001 to .0006
θ	1 to 0.2	8 to 0.8	17 to 10

In any case the correctness of the present calculations for the particular geometry chosen seems assured by the agreement of the results for $\underline{p}$ and $\underline{D}$ with other formulas in all of the limiting cases tried, except at large θ and $\underline{T}$. (See Appendix B for additional tests.)

The dashed curve of Figure 6 corresponds to $D(t)/\underline{D}(o)$ which one would calculate by plotting $\ln\underline{R}$ vs $\underline{g}^2$ at various $\underline{T}$, and estimating an average slope over the first decade of decrease in $\underline{R}$ to calculate $\underline{D}$. Since some arbitrariness was involved in deciding what is the average slope of a curved line, this dashed line is only approximate. It is presented because it resembles the procedure one would follow in treating real data. We note that it does not belong to the family of curves represented by the solid lines. This is because in actual experiments we tend to decrease θ as we increase $\underline{T}$, so as to prevent too much signal attenuation, whereas the solid lines are at constant θ .

The times at which $\underline{D}(\underline{t})$ reaches its arithmetic mean value are plotted in Figure 7 for each of several θ . Times for the arithmetic and geometric mean values at small θ are presented in Table 2. Also presented, in the last column of Table 2, is the fraction of particles outside the center layer at the time of geometric mean $D(t)$. The significance of these is discussed in the following two sections.

28
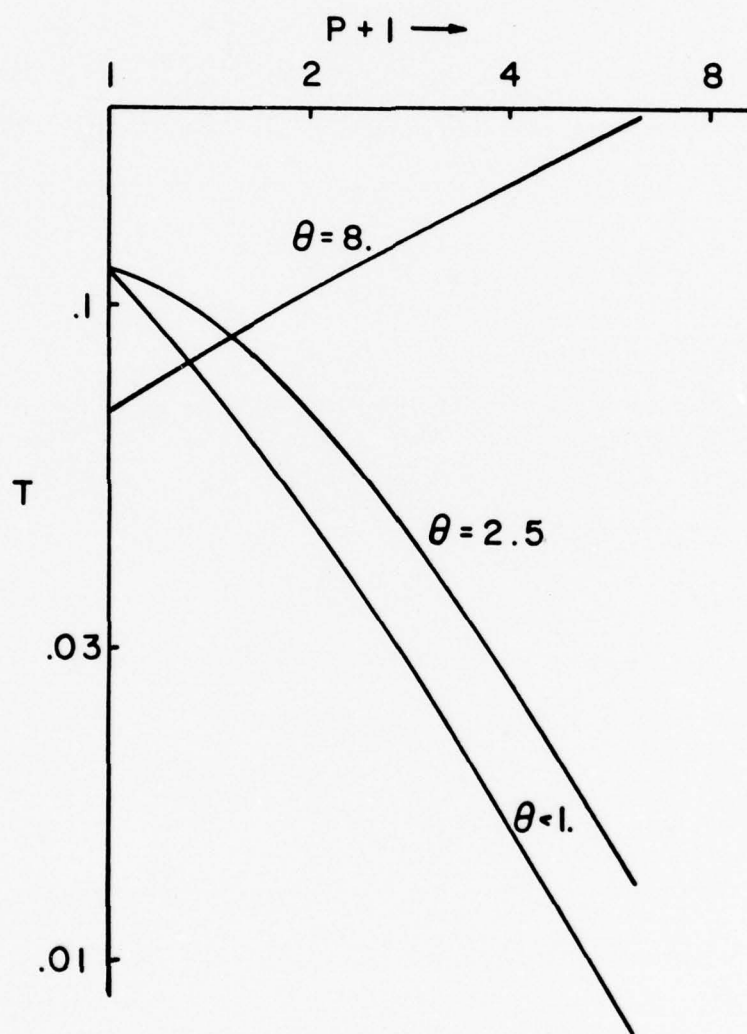
Fig. 7. Time at which the arithmetic average diffusion coefficient occurs, versus reduced permeability, for several values of θ.

TABLE II

Diffusion times and particle distributions corresponding to the mean
of the initial and final diffusion coefficients

P	$D(\infty)/D(o)$	At Arithmetic Mean D		At Geometric Mean D		
		D(mean)	T	D(mean)	T	$\int_{i\neq o}\rho dx$
5.	.833	.917	.0081	.910	.0105	.063
2.	.667	.833	.0257	.815	.035	.088
.5	.333	.667	.069	.577	.126	.099
.001	.001	.501	.113	.032	2.76	.0056

Physical Interpretation

It was initially expected that the time of mean $\underline{D}$ would not depend strongly on P. In that case it could have been said that the observation time required to detect the presence of barriers depended on their spacing, but not on their permeability. In other words, their effect would be proportional to the fraction of particles which had contacted them. We see from Figure 7 and Table 2 that this is not true.

It has also been proposed[12] that the restrictive effects are manifested in proportion to the fraction which have been reflected by the barriers. In that case the time of mean $\underline{D}(\underline{t})$ should increase with increasing $\underline{P}$. We see (Figs. 6 and 7) that just the opposite occurs.

The best qualitative description found is that the effects are manifested in proportion to the number of particles which have penetrated the barriers. This is illustrated in the last column of Table 2 by the nearly constant value of the fraction of particles outside their layer of origin at the time of mean $\underline{D}(\underline{t})$ for all but very low $\underline{P}$. Of course, such a criterion cannot even be applied to the case P = 0.

31

Evaluation Of Experimental Results

Thus far we have calculated apparent diffusion coefficients,
given barrier spacings and permeabilities, and intrabarrier diffusion
coefficients. In experimental situations we desire to do the reverse--
evaluate the barrier parameters and intrabarrier diffusion coefficient
from a set of apparent (measured) diffusion coefficients over a range
of diffusion times.

Although the actual geometry of the restrictive barriers may be
considerably different from parallel planes, it is believed that
an application of the results pertaining to small θ obtained for this
case should give a reasonably good approximation to the correct system
parameters.

Although it would be possible to fit a set of data to Eq.(8)
and extract $\underline{a}$, $\underline{P}$ and $D(o)$ by a non-linear regression procedure, this
would be costly. Instead, it is worth the trouble of extending the
range of diffusion times as far as possible, so that $\underline{D}(o)$ and $\underline{D}(\infty)$
can be estimated directly. The product $\underline{ap}$ can then be calculated
from Eq.(11). If $\underline{a}$ is not known from other information it may be
obtained from Figure 7, employing the curve for small θ .

SUMMARY

A general treatment of time-dependent (transient) diffusion
coefficients in a system containing barriers of arbitrary perme-
ability has been given. An exact expression in series form has been
obtained for the distribution function at arbitrary time, resulting
from one-dimensional diffusion originating at any point, and occurring
in a homogeneous medium containing equally spaced, planar barriers
of arbitrary but equal permeability. This function has been used
to calculate the time dependence of the diffusion coefficient as it
would be measured in pulsed gradient NMR experiments employing dif-
fusion times short enough so that few of the diffusing particles had
contacted the barriers, to times long enough so that most of them
had.

The time dependent diffusion coefficient was also calculated
using the Einstein formula $\underline{D(t)} = \overline{x^2}/2\underline{t}$. Numerical results of the
two methods agree in the limit where the applied field gradient is
zero. However, results obtained from the pulsed-gradient formula
are strongly dependent on the gradient when $\gamma\underline{g}\delta\underline{a}$ exceeds unity.

Numerical results for the distribution function and for diffusion
coefficients, covering a wide range of reduced diffusion times,
relative permeabilities, and field gradients are presented. From
the results it is shown how in many cases the reverse process of

33

evaluating these parameters from experimental diffusion data by hand calculation is possible.

It is suggested that the results should be approximately correct for other systems of repeated barriers. In the case of pulsed gradient NMR experiments this would mean colloidal systems such as biological tissues, interconnected pores in a rock, or the continuous phase of an emulsion.

REFERENCES

1. E. O. STEJSKAL, Adv. Mol. Rel. Processes $\underline{3}$, 27 (1972).

2. J. E. TANNER in <u>Magnetic Resonance in Colloidal and Interface Science</u>, ACS Symposium Series, No. 34, American Chemical Society (1976) ed. H. A. Resing and C. G. Wade, p 16.

3. C. H. NEUMAN, J. Chem. Phys. $\underline{60}$, 4508 (1974).

4. E. O. STEJSKAL, J. Chem. Phys. $\underline{43}$, 3597 (1965).

5. J. S. MURDAY and R. M COTTS, J. Chem. Phys. $\underline{48}$, 4938 (1968).

6. J. E. TANNER, PhD Thesis, University of Wisconsin (1966), obtainable from University Microfilms, Inc., Ann Arbor, Mich, No. 66-5951.

7. J. E. TANNER and E. O. STEJSKAL, J. Chem. Phys. $\underline{49}$, 1768 (1968).

8. B. ROBERTSON, Phys. Rev. $\underline{151}$, 273 (1966).

9. R. C. WAYNE and R. M. COTTS, Phys. Rev. $\underline{151}$, 264 (1966).

10. R. L. COOPER, D. B. CHANG, A. C. YOUNG, C. J. MARTIN, and B. ANCKER-JOHNSON, Biophys. J. $\underline{14}$, 161 (1974).

11. E. O. STEJSKAL and J. E. TANNER, J. Chem. Phys. $\underline{42}$, 288 (1965).

12. M. N. OZISIK, <u>Boundary Value Problems of Heat Conduction</u>, (International Textbook Co., Scranton, Pa., 1968) Chap 6.

13. G. P. MULHOLLAND and M. H. COBBLE, Int. J. Heat Mass Transfer $\underline{15}$, 147 (1972).

APPENDIX A

NOTES ON THE CALCULATIONS

The Eigenfunctions of ρ

The roots, β , of the matrix of boundary equations used to determine the eigenfunctions from which ρ is constructed, occur in groups of $\underline{m}$, where m is the number of layers in the system. Each group begins approximately at an integral multiple of π . The spacing within a group increases as larger values of P are selected. For $\underline{P}=\infty$ we have $\beta_{\underline{n}}=\underline{n}\pi/\underline{m}$.

The computer time required is approximately proportional to m^2, because the number of β required, and the time required to evaluate the sparse matrix, each increase linearly with $\underline{m}$. Most of the time is used in evaluating the $\beta_{\underline{n}}$. Once this is done for a give $\underline{P}$, then ρ and $\underline{D}(\underline{t})$ (by Eq. (2) or (4)) may be calculated quickly for a large number of locations or times, respectively. As a typical example for a 19-layer system, the time required to evaluate 266 values of β (the usual number of terms) to double precision accuracy (single precision would have sufficed), and subsequently evaluate D by Eqs. (2) and (4), at four values of θ , each at 70 values of $\underline{T}$, was 70 sec. on a CDC 6600 computer.

Listing of the various programs are available on request.

APPENDIX B

ADDITIONAL CHECKS

Several additional checks on the correctness of the results are as follows:

It was found that $\underline{R}=1$ for $\Theta=0$ for all $\underline{T}$ up to where the outer boundaries become important. This was done at several $\underline{P}$.

$\underline{D}(\underline{t})/\underline{D}(o)$ was calculated directly from ρ by a Simpson rule integration of Eq.(2). This was done at several $\underline{P}$ and several $\underline{T}$, for $\Theta>1$. The results were identical to those obtained from Eq.(8) to the number of significant figures printed out.

Equation (8) was rederived from Eqs. (2) and (5) using two other coordinate systems. In one case a single origin for $\underline{x}$ and $\underline{x}_o$ was located at an outer boundary. In the other case a single origin was located at the center of the center layer. Numerical results were in agreement with those for the coordinate system described earlier for all values calculated, to within the 4-6 significant figures printed out.

Distribution functions and diffusion coefficients calculated for $\underline{P}=0$ agreed to the number of figures printed out, over the entire time range, with the results[8,9] which had been obtained earlier for this special case using a different formula.

37

A few calculations were performed with a 41-layer system, so as to extend the range to longer T. However, D continued to decrease with increasing T for all Θ used. All calculations of ρ or D agreed among systems of varying number of layers, provided the comparison was at times short enough so that ρ was negligible in the outermost layers of the smallest system considered.

DISTRIBUTION LIST

ADDRESS	COPIES
Administrator, Defense Documentation Center Cameron Station Alexandria, Virginia 22314	12
Director, Naval Research Laboratory Attention: Technical Information Division Code 2027 Washington, D.C. 20390	6
Director, Naval Research Laboratory Attention: Library Code 2029 (ONRL) Washington, D.C. 20390	6
Office of Naval Research Medicine and Dentistry Code 444 Arlington, Virginia 22217	3
Director, Research Division Bureau of Medicine and Surgery Department of the Navy Washington, D.C. 20390	2
Technical Reference Library Naval Medical Research Institute National Naval Medical Center Bethesda, Maryland 20014	2
Office of Naval Research Branch Office 495 Summer Street Boston, Massachusetts 02100	1
Office of Naval Research Branch Office 536 South Clark Street Chicago, Illinois 60605	1
Office of Naval Research Branch Office 1030 East Green Street Pasadena, California 91101	1
Office of Naval Research Contract Administrator for Southeastern Area 2110 G. Street, N.W. Washington, D.C. 20007	1

DISTRIBUTION LIST (cont.)

ADDRESS	COPIES

Commanding Officer
U.S. Naval Medical Research Unit No. 2
Box 14
APO San Francisco 96263 1

Commanding Officer
U.S. Naval Medical Research Unit No. 3
FPO New York 09527 1

Officer in Charge
U.S. Naval Medical Research Unit No. 4
U.S. Naval Hospital
Great Lakes, Illinois 60088 1

Commanding Officer
Naval Submarine Medical Research Laboratory
Naval Submarine Base, New London
Groton, Connecticut 06340 1

Scientific Library
U.S. Naval Medical Field Research Laboratory
Camp Lejeune, North Carolina 28542 1

Scientific Library
Naval Aerospace Medical Research Institute
Naval Aerospace Medical Center
Pensacola, Florida 32512 1

Commanding Officer
Naval Air Development Center
Attention: Aerospace Medical Research Department
Johnsville, Warminster, Pennsylvania 18974 1

Scientific Library
Naval Biomedical Research Laboratory
Naval Supply Center
Oakland, California 94625 1

Director, Life Sciences Division
Army Research Office
3045 Columbia Pike
Arlington, Virginia 22204 1

Director, Life Sciences Division
Air Force Office of Scientific Research
1400 Wilson Boulevard
Arlington, Virginia 22209 1

DISTRIBUTION LIST (cont.)

<u>ADDRESS</u>   <u>COPIES</u>

Commanding General
U.S. Army Medical Research & Development Command
Forrestal Building
Washington, D.C. 20314   1

Commander
Naval Air Systems Command
Department of the Navy
Washington, D.C. 20361
Attention: Code AIR-954, Technical Library   2
             Code AIR-310C, Dr. H. Rosenwasser   1

Commander
Naval Sea Systems Command
Naval Sea Systems Command Headquarters
Washington, D.C. 20362
Attention: Code SEA-09G3, Technical Library   2
             Code SEA-0332, Dr. A. B. Amster   1

Commander
Naval Weapons Center
China Lake, California 93555
Attention: Code 533, Technical Library   2
             Code 60, Dr. H. W. Hunter   1

Commander
Air Force Avionics Laboratory
Wright-Patterson Air Force Base
Ohio 45433
Attention: Code AFAL/CC   1

Officer in Charge
White Oak Laboratory
Naval Surface Weapons Center
Silver Spring, Maryland 20910
Attention: Code 230, Dr. L. A. Kaplan   1
             Code WR-20, Dr. W. McQuistion   1
             Code WX-21, Technical Library   1

41

DISTRIBUTION LIST (cont.)

<u>ADDRESS</u>   <u>COPIES</u>

Commander
Army Aviation Systems Command
Avionics and Weaponization Division
St. Louis, Missouri 63166
Attention: Code DRSAV-EVW   1

Commanding General
U.S. Army Tank Automotive Command
Warren, Michigan 48090
Attention: Code DRSTA-RHFL   1

Commander
Naval Surface Weapons Center
Dahlgren Laboratory
Dahlgren, Virginia 22448
Attention: Code DG-50, Mr. R. Morrissette   1

Commanding Officer
Frankford Arsenal
Philadelphia, Pennsylvania 19173
Attention: Code SARFA-MDP-Y, Mr. W. Puchalski   1

Commanding Officer
Edgewood Arsenal
Aberdeen Proving Ground, Maryland 21010
Attention: Code SAREA-DE-MMP, Mr. M. Penn   1

Commander
Ballistic Research Laboratories
Interior Ballistics Laboratory
Aberdeen Proving Ground, Maryland 21005
Attention: Code DRXBR-IB, Mr. J. R. Ward   1

Commander
Aeronautical Systems Division (AFSC)
Wright-Patterson Air Force Base
Ohio 45433
Attention: Code ASD/ENAMC, Mr. M. Edelman   1

Commander
Army Armament Research and Development Command
Dover, New Jersey 07801
Attention: Code DRDAR-LCE-T, Mr. T. Boxer   1
            Code DRDAR-LCE-T, Dr. F. Taylor   1
            Code DRDAR-TSS, Technical Library   1

ADDRESS	COPIES
Commander Armament Development and Test Center Eglin Air Force Base Florida 32542 Attention: Code ADTC/SD3E	1
Commander Air Force Armament Laboratory Eglin Air Force Base Florida 32542 Attention: Code AFATL/DLJW, Mr. A. Beach	1
Commanding Officer Naval Ordnance Station Indian Head, Maryland 20640	1
Commander Rome Air Development Center Griffiss Air Force Base New York 13441	1
The Johns Hopkins University Applied Physics Laboratory 8621 Georgia Avenue Silver Spring, Maryland 20910 Attention: Library Acquisitions: Bldg. 5, Rm. 26	1
Environmental Research Institute of Michigan P.O. Box 8618 Ann Arbor, Michigan 48107 Attention: IRIA Library	1
Battelle Memorial Institute TACTEC Columbus, Ohio 43201 Attention: Ms. Nancy Hall	1
National Aeronautics and Space Administration Langley Research Center Hampton, Virginia 23665	1
National Aeronautics and Space Administration Lewis Research Center 21000 Brookpark Road Cleveland, Ohio 44135	1

DISTRIBUTION LIST (cont.)